Moroccan Journal of Chemistry
ISSN: 2351-812X
http://revues.imist.ma/?journal=morjchem&page=login
Ushaka & al. / Mor. J. Chem. 9 N°4 (2021) 677-696
DOI: https://doi.org/10.48317/IMIST.PRSM/morjchem-v9i3.22346

Quantum and Electrochemical Studies of Corrosion Inhibition Impact on Industrial Structural Steel (E410) by Expired Amiloride Drug in 0.5 M Solutions of HCl, H_2SO_4 and $NaHCO_3$

B. U. Ugi,[(a)]*, [2]M. E. Obeten[(b)], V. M. Bassey[(a)], E. J. BoEkom[(c)], E. C. Omaliko[(a)], F. B. Ugi[(d)], I. E. Uwah[(a)]

[(a)] Department of Pure & Applied Chemistry, University of Calabar, P. M. B. 1115, Calabar – Nigeria.
[(b)] Department of Chemistry, Cross River State University of Technology, Calabar – Nigeria
[(c)] Department of Chemistry, University of Uyo, P. M. B. 1017, Uyo – Nigeria
[(d)] Department of Chemical & Petrochemical Engineering, River State University of Science & Technology, Port Harcourt – Nigeria

** Corresponding author:*
ugibenedict@gmail.com
Received 11 Aug 2020,
Revised 02 Nov 2021,
Accepted 04 Nov 2021

Abstract

Computational and Electrochemical Studies of Corrosion Inhibition Impact on Industrial Structural Steel (E410) by Expired Amiloride Drug in 0.5 M Solutions of HCl, H2SO4 and NaHCO3 was carried out under the following experimental and analytical methods: Mass loss, thermometric, electrochemical impedance spectroscopy, potentiodynamic polarization, Quantum chemical calculations, simulation analysis and scanning electron microscopy (SEM). Findings revealed that the inhibitor is highly effective in all the tested media with surface coverage and an inhibition efficiency of 0.99/98.6, 0.92/92.2 and 0.88/88.2 % for HCl, H2SO4 and NaHCO3 respectively. Electrochemical data revealed strong adsorption of the inhibitor in both solutions as charged transfer resistance as in the increased. Thermodynamically, the inhibitor was stabled, spontaneous, physically adsorbed and associative. The theoretical data showed an energy gap of 0.019 eV close enough to allow speedy movement of the inhibitor molecules across energy levels. A good correlation of the data was found with the Langmuir isotherm compared to the El-Awady, hence a monolayer chemical adsorption as deduced. The electrochemical, SEM and theoretical data were in agreement with those of chemical experiment confirming expired amiloride as a good inhibitor of industrial structural steel (E410) in 0.5 M solutions of HCl, H_2SO_4 and $NaHCO_3$.

Keywords: *Amiloride, polarization, impedance, inhibition, adsorption.*

1. Introduction

Industrial structural steel is twice as strong as commercial steel and is a steel used in heavier and more complex applications and also where heat and other environmental factors can degrade less durable metals especially in the Oil platforms and other industrial settings [1 -2] . One can also find industrial structural steel in areas requiring metals that can withstand pressure, high temperatures, rust, chemicals and erosion. It is more expensive than commercial steel, and unlike commercial steel, industrial steel is not easy to weld. It is thicker and heavier and is more prone to both cracking and lamellar tears. Even small notches from access holes and the stress from welding enable cracks to form and propagate hence making the metal susceptible to both pitting and intergranullar corrosion attacks. Application of industrial steel is found in construction, vessels and Aircraft, Pipelines, Wind turbine, etc. [1-2].

Corrosion of metals has embraced a whole lot of damages from within the metal applied sector and outside the metal-based environments. Corrosion which is seen to be emphatically an electrochemical based reaction process with sometimes even a chemical and acid based process inclusive, has effects on industrial and commercial structures like churches, office buildings, banks, retail buildings, aircrafts, constructions – cars, heavy duty machines, etc. [3-4]. It is always identified with deterioration of metal surfaces as a result of interaction with environments exposed to moisture and air, that is, an anodic – cathodic electrode based reaction with centrality in the nature of electrolyte involved [5-7]. Different corrosion processes based on type can always be identified with either of commercial or industrial steel. These forms of corrosion always start with pitting corrosion and then advanced to either granular, crevice, concentration cell, galvanic, etc. the possible oxidation at the anodic sites of a metal due to lose in electron and corresponding cathodic site hydrogen gas evolution always give rise to corrosion emergence [5, 8-10]. Inhibitors are employed as a means of checking the excessiveness of metal corrosion within specified environmental conditions [8-9]. Inhibitors could be organic or inorganic, or they could be green and eco-friendly or toxic. The pursuit for an eco-friendly inhibitor lead to the dominant research in the use of both synthesized plant extracts or drugs (expired or active) in the combat of corrosion in virtually all medium but most importantly in acidic media. The frequent choice of acidic media originates from the regular use of these acids in industrial pickling, cleansing, scale removal, and so on [11-12]. Inhibitors, more often act by dominating the surface of the metal through adsorption on active sites of the metal that lead to oxidation or reduction to some extent and possible corrosion incidence. This is always possible with green inhibitors that possesses hetero-compounds (alkaloids, flavonoids, tannins, saponins, etc.) or hetero-atoms like sulphur (S), phosphorus (P), Nitrogen (N), or pie bond from the presence of double or triple bond, aromaticity, etc [9, 13-14]. The choice of expired amiloride drug comes from its abundance in this part of the country due to the believe in traditional medicine (which of course works for them), the inability of negative drug adjustment by front line health workers and pharmacist and the many options available for the treatment of high blood pressure based on drug reaction effects. Amiloride is a synthetic pyrazine derivative with antikaliuretic and diuretic properties (Fig. 1).

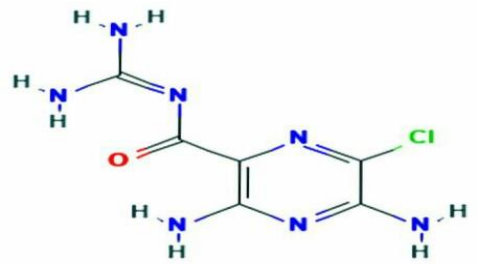

Figure. 1 Chemical structure of Amiloride

It's a medication typically used with other medications to treat high blood pressure or swelling due to heart failure. Amiloride inhibits sodium channels located in the distal tubules and collecting ducts of the kidney through reduction of electrochemical forces, thereby preventing the absorption of sodium, excretion of hydrogen and potassium and increasing its excretion along with water. Ceaseless action of corrosion is a burden on national wealth. Approximately 1 ton of steel is converted to rust every 90 seconds in Nigeria and 50 % of steel produced is used to replace corroded steel [15]. The world is becoming more and more intolerant to health and safety hazards caused by upland hydrocarbon discharges. At least 25 % of corrosion lost can be prevented by appropriate action – choice of proper corrosion maintenance method (s) and control measures. It is on this basis that the researcher are undertaking the research on the Corrosion Inhibition Impact on Industrial Structural Steel (E410) by Expired Amiloride Drug in 0.5 M Solutions of HCl, H2SO4 and NaHCO3.

2. Materials and methods

2.2 Metal preparation and preservation

The industrial constructional steel was acquired from System Metals Nig. Limited and with a composition of Fe (98.34%) C (0.19%), Si (0.26%), Na (0.64%), S (0.05%), P (0.06%), Ni (0.09%), Cr (0.08%), Mo (0.02%), and Cu (0.27%). The industrial constructional steel was then resized into coupons of dimension 5.0 x 1.8 x 3.0 cm for mass loss analysis, 2.5 x 0.08 x 2.5 cm for thermometric analysis and 1 x 1 cm for electrochemical studies, at the Physics Department Workshop of the University of Calabar. The coupons were subsequently descaled by polishing to mirror surface using different grades of emery papers from coarse to extra fine (120, 220 and 1200) grits in an electronic UNIPOL- 820 metallographic polishing machine. This was changed regularly to avoid clogging. The polished coupons were now washed with distilled water, rinsed in ethanol, degreased with Acrastrip 600 Auto reagent and air dried and stored in a desiccator prior to use.

2.3 Thermometric (Heat) analysis

Thermometry is by far the simplest thermal analysis technique involving the measurement of temperature and usually the measurement of time. Here, the prepared metal coupons of dimension 2.5 x 0.08 x 2.5 cm were at different occasion allowed into a solution of 0.5 M HCl, H_2SO_4 and $NaHCO_3$ and immersed in a regulated water bath at temperatures of 303, 318, 323 and 338 for 60 min each. The metal coupon was retracted from the solution, washed with distilled water, rinsed in ethanol, degreased with Acrastrip 600 Auto reagent and air dried then weighed. This procedure was repeated for the various concentrations and different temperatures until the entire experiment was completed for all the media. The surface coverage and % inhibition efficiency of inhibitor was determined from **Equation 1 and 2**

$$\text{Surface coverage } (\Im) = \frac{(Cr_x - Cr_y)}{Cr_x} \quad (1)$$

$$\text{Inhibition efficiency } (\%\,\wp) = \left[1 - \frac{Cr_y}{Cr_x}\right] x100 \quad (2)$$

where $\Im$ is the surface coverage of inhibitor, Cr_x and Cr_y are the corrosion rates of the free and inhibited solutions, $\%\,\wp$ is the percentage inhibition efficiency of the inhibitor.

2.4 Mass loss analysis

This is the most reliable chemical method for the determination of corrosion rate of a metal and the inhibition efficiency of the inhibitor. Using this method, the polished and dressed coupons of dimension 5.0

x 1.8 x 3.0 cm were initially weighed and readings recorded. They were then immersed in the individual free solutions of 0.5 M HCl, H_2SO_4 and $NaHCO_3$ daily for 5 days (120 hrs). The coupons were then removed from the solutions, washed with distilled water, rinsed in ethanol, degreased with Acrastrip 600 Auto reagent and air dried then re-weighed. This procedure was repeated for the various concentrations on till the entire experimentation was completed for all the media. The surface coverage and % inhibition efficiency of inhibitor was determined from **equation 3 and 4**

$$\text{Surface coverage } (\Im) = \frac{(Cr_x - Cr_y)}{Cr_x} \quad (3)$$

$$\text{Inhibition efficiency } (\%\,\wp) = \frac{(Cr_x - Cr_y)}{Cr_x} x100 \quad (4)$$

where $\Im$ is the surface coverage of inhibitor, Cr_x and Cr_y are the corrosion rates of the free and inhibited solutions, $\%\,\wp$ is the percentage inhibition efficiency of the inhibitor.

2.5. Electrochemical method (EIS/PDP)

The EIS was carried out in triple electrode cell circuit using Gamry Reference 600 potentiostart/galvanostart inclusive of a Gamry framework EIS300 system. The fitting of the data was analyzed using the Echem analyst software. The reference electrode for the system was a saturated calomel (SCE) electrode and a $1cm^2$ platinum foil was adopted as a counter electrode. The working electrode (industrial structural steel coupon) with dimension 1 cm x 1 cm was dipped in 0.5 M HCl, H_2SO_4 and NaHCO3 at different intervals. Electrochemical tests were conducted within a frequency of 10 Hz - 100,000 Hz within Potentiodynamic conditions, with an amplitude of 5 mV, involving alternating current signal at E_{corr}. The Potentiodynamic polarization measurement was carried out by altering the electrode potential from – 0.15 to + 0.15 V with respect to OCP at a scan rate of 0.2 mV/s. The data for corrosion density (I_{corr}) and corrosion potential (E_{corr}) were acquired automatically using Versa Studio software. All experiments were conducted every 60 min with the free and inhibited solutions. From the ϕ_{ct}^0 and I_{corr} obtained, the surface coverage and inhibition efficiencies was calculated using **Equation 5 – 7** respectively:

$$\Im = \frac{\phi_{ct}^0 - \phi_{ct}^i}{\phi_{ct}^0} \quad (5)$$

$$\%\,\wp = \frac{\phi_{ct}^0 - \phi_{ct}^i}{\phi_{ct}^0}\, x\, 100 \quad (6)$$

$$\%\,\wp = 100\left[1 - \frac{I_{corr}^i}{I_{corr}^0}\right] \quad (7)$$

where $\Im$ is the surface coverage of the inhibitor, ϕ_{ct}^0 and ϕ_{ct}^i represent the charge transfer resistance and I_{corr}^0 and I_{corr}^i is the corrosion density in the free and inhibited solutions of amiloride inhibitor respectively.

2.6 Computational method

The basic methodology employed in this analysis is the quantum chemical calculations and molecular dynamics simulation analysis. This was carried out using a software Material Studio (version 8.0) from Accelyrs Inc. San Diego Califonia, United States of America installed on a Personal Computer. The quantum chemical calculations were conducted using two (2) programs - the Vamp and Dmol^3. The Vamp is a highly efficient semi-empirical molecular orbital package, theoretical calculations were carried out at the Restricted Hartree-Fock level (RHF) using the Hamiltonian parametric method 3 (PM3), which is based on the neglect of diatomic differential overlap approximation. The Dmol^3 is a program which make use of the

density functional theory (DFT) with a numerical radial function basis set to calculate the electronic properties of molecule's clusters. Information obtained include higher occupied molecular orbital energy (E_{HOMO}), lower unoccupied molecular orbital energy (E_{LUMO}), Fukui positive and negative indices plots, HOMO and LUMO energy plots, energy gap (ΔE), chemical potential (μ), global hardness (η) and global softness (S), electrophilicity index (ω), according to **equation 8 – 12** respectively.

$$\text{Energy gap } (\Delta E) = E_{HOMO} - E_{LUMO} \quad (8)$$

$$\text{Chemical potential } (\mu) = -\frac{(E_{HOMO} + E_{LUMO})}{2} \quad (9)$$

$$\text{Global hardness } (\eta) = \frac{(E_{HOMO} - E_{LUMO})}{2} \quad (10)$$

$$\text{Global softness } (S) = \frac{1}{2\left[\frac{(E_{HOMO} - E_{LUMO})}{2}\right]} \quad (11)$$

$$\text{Electrophilicity index } (\omega) = \frac{\mu^2}{2\left[\frac{(E_{HOMO} - E_{LUMO})}{2}\right]} \quad (12)$$

2.7 Scanning electron microscopy

The surface analysis of the inhibitor on the industrial structural steel coupons at the free solutions (0.5 M) and highest inhibitor concentration (7.0 x 10^{-3} M) was determined through the aid of Phenom Pro Scanning electron microscope (**Figure. 2**). The Phenom Pro is Phenom-World's high-end imaging desktop SEM. In combination with a large range of sample-holders and automated system software, it can be tailored to suit a multitude of applications. 10 kV acceleration voltage was maintained for outstanding high-resolution SEM images.

Figure 2. Phenom Pro Scanning electron microscope

3. Results and Discussion

3.1 Thermometric results and interpretation

Data for the influence of temperature rise on the potentials of the expired amiloride inhibitor on the industrial structural steel coupons in various test media is displayed in Tables 1 - 3. Result showed that the inhibition was highly significant at lower temperatures for all test media compared to the highest temperature. This is likely to be the temperature agitation effect on the inhibitor, consequent upon its loosely bonded atoms [12, 14-16]. The inhibition efficiency was increasing with increased inhibitor concentration but decreasing with rise in temperature. This was an indication of stronger molecular adsorption following increased inhibitor concentration [16]. Also this tendency can be attributed to a physical adsorption process by the inhibitor on the metal surface and temperature dependent. It was also noticed that across various temperatures, the inhibitor was found to have possessed a stronger adsorption in the presence of HCl acid, followed by NaHCO3 and then H2SO4. This could be attributed to the basicity of the test solutions since acid strength is always defined by their basicity and higher corrosion rate is well expected from acid of higher basicity [17-18].

Table 1: Thermometric data revealing corrosion rate (Cr), surface coverage (ϑ) and inhibition efficiency (% ℘) for the corrosion inhibition of industrial structural steel coupons in 0.5 M HCl solutions.

Inhibitor Conc.	Cr (mg/cm²/min)				(ϑ)				(% ℘)			
	303K	318K	323K	338K	303K	318K	323K	338K	303K	318K	323K	**338K**
0.5M HCl	12.962	17.828	28.154	37.038	-	-	-	-	-	-	-	-
1.0 x 10-3 M	5.027	7.296	13.439	19.298	0.61	0.59	0.52	0.48	61.2	59.1	52.3	**47.9**
1.5 x 10-3 M	2.835	6.104	12.195	17.672	0.78	0.66	0.57	0.52	78.1	65.8	56.7	**52.3**
2.0 x 10-3 M	2.319	4.783	11.274	15.834	0.82	0.73	0.60	0.57	82.1	73.2	60.0	**57.2**
3.5 x 10-3 M	1.034	2.142	5.267	9.016	0.92	0.88	0.81	0.76	92.0	88.0	81.3	**75.7**
5.0 x 10-3 M	0.597	1.821	3.846	6.044	0.95	0.90	0.86	0.84	95.4	89.8	86.3	**83.7**
7.0 x 10-3 M	0.103	1.001	2.743	4.243	0.99	0.94	0.90	0.89	99.2	94.4	90.3	**88.5**

Table 2: Thermometric data revealing corrosion rate (Cr), surface coverage (ϑ) and inhibition efficiency (% ℘) for the corrosion inhibition of industrial structural steel coupons in 0.5 M **$NaHCO_3$** solutions.

Inhibitor Conc.	Cr (mg/cm²/min)				(ϑ)				(% ℘)			
	303K	318K	323K	338K	303K	318K	323K	338K	303K	318K	323K	**338K**
0.5M $NaHCO_3$	9.453	15.269	19.190	23.718	-	-	-	-	-	-	-	-
1.0 x 10-3 M	4.046	6.920	9.724	12.475	0.57	0.55	0.49	0.47	57.20	54.7	49.3	**47.4**
1.5 x 10-3 M	2.154	5.921	8.945	11.785	0.77	0.61	0.53	0.50	77.2	61.2	53.4	**50.3**
2.0 x 10-3 M	2.001	4.529	7.911	10.749	0.79	0.70	0.59	0.55	78.8	70.3	58.8	**54.7**
3.5 x 10-3 M	1.101	2.094	5.278	8.638	0.88	0.86	0.72	0.64	88.4	86.3	72.5	**63.6**
5.0 x 10-3 M	0.748	1.948	3.527	5.119	0.92	0.87	0.82	0.78	92.1	87.2	81.6	**78.4**
7.0 x 10-3 M	0.319	1.423	2.936	3.903	0.97	0.91	0.85	0.84	96.6	90.7	84.7	**83.5**

Table 3: Thermometric data revealing corrosion rate (Cr), surface coverage (ϑ) and inhibition efficiency (% ℘) for the corrosion inhibition of industrial structural steel coupons in 0.5 M **H_2SO_4** solutions.

Inhibitor Conc.	Cr (mg/cm²/min)				(ϑ)				(% ℘)			
	303K	318K	323K	338K	303K	318K	323K	338K	303K	318K	323K	**338K**
0.5M H_2SO_4	15.298	22.019	30.647	41.385	-	-	-	-	-	-	-	-
1.0 x 10-3 M	8.274	12.840	19.047	26.004	0.46	0.42	0.38	0.37	45.9	41.7	37.9	**37.2**
1.5 x 10-3 M	7.157	11.586	17.264	25.000	0.53	0.47	0.44	0.40	53.2	47.4	43.7	**39.6**
2.0 x 10-3 M	6.879	10.631	16.600	22.846	0.55	0.52	0.46	0.45	55.0	51.7	45.8	**44.8**
3.5 x 10-3 M	4.745	8.455	13.819	18.511	0.69	0.62	0.55	0.55	69.0	61.6	54.9	**55.3**
5.0 x 10-3 M	2.861	5.108	10.435	15.037	0.81	0.77	0.66	0.64	81.3	76.8	66.0	**63.7**
7.0 x 10-3 M	1.950	3.617	6.276	11.174	0.87	0.84	0.80	0.73	87.3	83.6	79.5	**73.0**

3.2 Mass loss results and interpretation

The amount of industrial structural steel coupon lose to the various test media at different concentration was determined using mass loss experiment and result obtained are displayed in **Table 4.** It was noticed that the m amount of metal loss to all the media was seen decreasing with increasing concentration of the inhibitor applied. This could be due to the strong adsorption of the inhibitor molecules due to bonding of molecules on the metal surface [15-16]. The surface coverage of the inhibitor was found to follow the progression HCl (0.986) > $NaHCO_3$ (0.922) > H_2SO_4 (0.882) indicating that the inhibitor had a good performance in HCl compared to other media hence forming a stronger intermolecular force of attraction at the inhibition-metal interface [18-20].

Table 4: Values of corrosion rate (Cr), surface coverage ($\Im$) and inhibition efficiency ($\%\wp$) for the corrosion inhibition of industrial structural steel coupons in 0.5 M HCl, $NaHCO_3$ and H_2SO_4 solutions analyzed from mass loss experiment.

	HCl			$NaHCO_3$			H_2SO_4		
Inhibitor Conc.	Cr (mg/cm^2/Hr)	$\Im$	$\%\wp$	Cr (mg/cm^2 /Hr)	$\Im$	$\%\wp$	Cr (mg/cm^2 /Hr)	$\Im$	$\%\wp$
Blank (0.5M)	7.2743			5.2873	-	-	2.1955	-	-
1.0 x 10-3 M	2.1944	0.6983	69.83	2.1736	0.5889	58.89	1.0005	0.5443	**54.43**
1.5 x 10-3 M	1.9261	0.7352	73.52	1.8389	0.6522	65.22	0.8593	0.6086	**60.86**
2.0 x 10-3 M	1.0284	0.8586	85.86	1.0489	0.8016	80.16	0.5517	0.7487	**74.87**
3.5 x 10-3 M	0.6204	0.9147	91.47	0.7399	0.8601	86.01	0.4537	0.7934	**79.34**
5.0 x 10-3 M	0.3683	0.9494	94.94	0.4652	0.9120	91.20	0.2719	0.8762	**87.62**
7.0 x 10-3 M	0.1024	0.9859	98.59	0.4112	0.9222	92.22	0.2598	0.8817	**88.17**

3.3 Electrochemical analysis and result (EIS)

Data for the electrical interference of the system with the inhibitor are presented in **Table 5** and the corresponding Nyquist plots are shown in **Figure. 5.** It was observed that the inhibitor presented a single capacity loop which is directed towards a single charge transfer [21-22]. Also, the size of these loops increases with the rise in expired amiloride concentration up to 7.0 x 10-3 M which is in line with the increased charge transfer values indicating an adsorption of the inhibitor and reduction of the exposed area of the metal to the test media [20, 22-23]. The data for the double-layer capacitance of the semicircle and inhibition efficiency were determined following **Equation 13 - 15** and are presented in **Table 5**

$$C_{dl} = \frac{1}{\omega Z''} \quad (13)$$

where Z'' is immaginay component of impedance at any frequency inside the semicircle ans ω is the angular frequency.

But $\omega = 2 * \pi * f_{max}$ (in Hz used for measurement of EIS).

Hence,

$$C_{dl} = \frac{1}{2\pi f_{max} Z''} \quad (14)$$

where f_{max} describe the maximun frequency of the semicircle and the π is 3.142.

$$\% \wp = \frac{\mathscr{b}_{ct}^{0} - \mathscr{b}_{ct}^{i}}{\mathscr{b}_{ct}^{0}} x\ 100 \qquad (15)$$

where $\mathscr{b}_{ct}^{0}$ and $\mathscr{b}_{ct}^{i}$ correspond to the charge ransfer values in the free and inhibited solutions of expired amiloride inhibitor respectively. The double layer capacitance values were decreasing while the inhibition efficiency values were increasing with progression in concentration. This follows that the charge metal interface / expired amiloride inhibitor solution witness a proper distribution of ionic charges, which suggests that the inhibitor acted very good hence the increase in inhibition efficiency as recorded [21, 24].

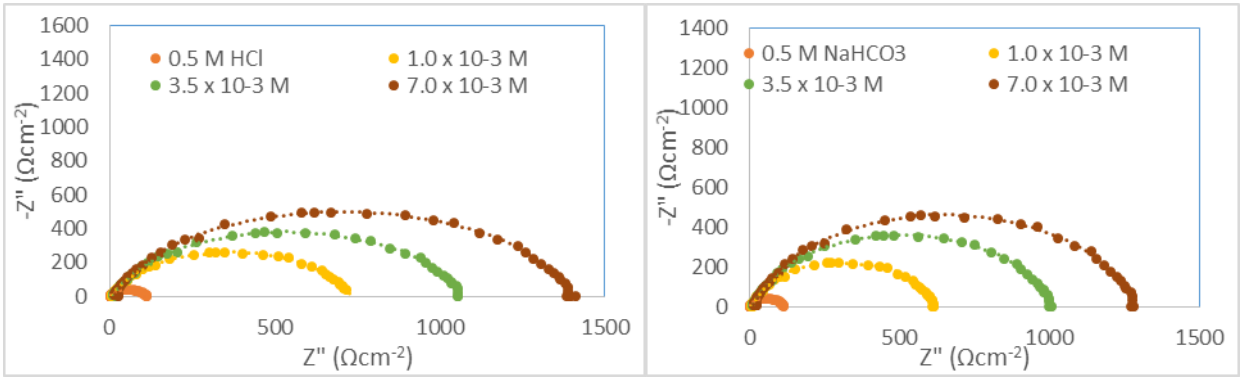

(a) *(b)*

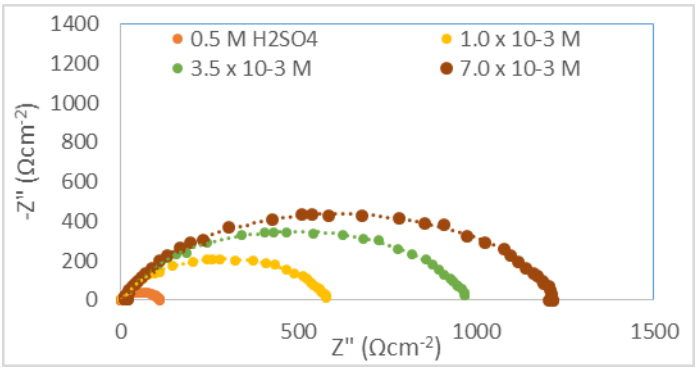

(c)

Figure 3. Nyquist plots for inhibition of industrial structural steel coupons in 0.5 M (a) HCl, (b) **$NaHCO_3$ and (c) H_2SO_4** solutions.

3.4 Electrochemical analysis and result (PDP)

Table 6 showed values of corrosion current density, corrosion potential, anodic and cathodic slopes and inhibition efficiency deduced from **Figure 4** There is an indication from the presented values that the expired amiloride inhibitor proved to be an efficient inhibitor against the industrial structural steel in both tested media but with a more reliable influence in the HCl medium. It was also confirmed that the corrosion potential values were shifted gradually to a more positive direction at every addition of inhibitor molecules, and also shows changes in both the cathodic and anodic polarization branches. This as an indication that the added expired amiloride molecules acted majorly as a mixed type inhibitor [23-25]. This can also be confirmed from the anodic and cathodic Tafel slope values in **Table 6**.

Table 5: Nyquist plots parameters showing data for inhibition of industrial structural steel coupons in 0.5 M HCl, **$NaHCO_3$ and H_2SO_4** solutions.

Inh. Conc.	R_{ct}	C_{dl}	ΘR_{ct}	ΘC_{dl}	$\%IER_{ct}$	$\%IEC_{dl}$
0.5 M HCl	105	1.5E-05	-	-	-	-
1.0 x 10^{-3}M	792	2.0E-06	0.867	0.860	86.7	86.6
3.5 x 10^{-3}M	1085	1.5E-06	0.903	0.900	90.3	90.0
7.0 x 10^{-3}M	1450	1.1E-06	0.928	0.926	92.8	92.6
0.5 M $NaHCO_3$	105	1.5E-05				
1.0 x 10^{-3}M	618	2.6E-06	0.830	0.826	83.0	82.6
3.5 x 10^{-3}M	946	1.7E-06	0.889	0.886	88.9	88.6
7.0 x 10^{-3}M	1300	1.2E-06	0.919	0.920	91.9	92.0
0.5 M H_2SO_4	105	1.5E-05				
1.0 x 10^{-3}M	511	3.1E-06	0.795	0.793	79.5	79.3
3.5 x 10^{-3}M	826	1.9E-06	0.873	0.873	87.3	87.3
7.0 x 10^{-3}M	1138	1.4E-06	0.908	0.906	90.8	90.6

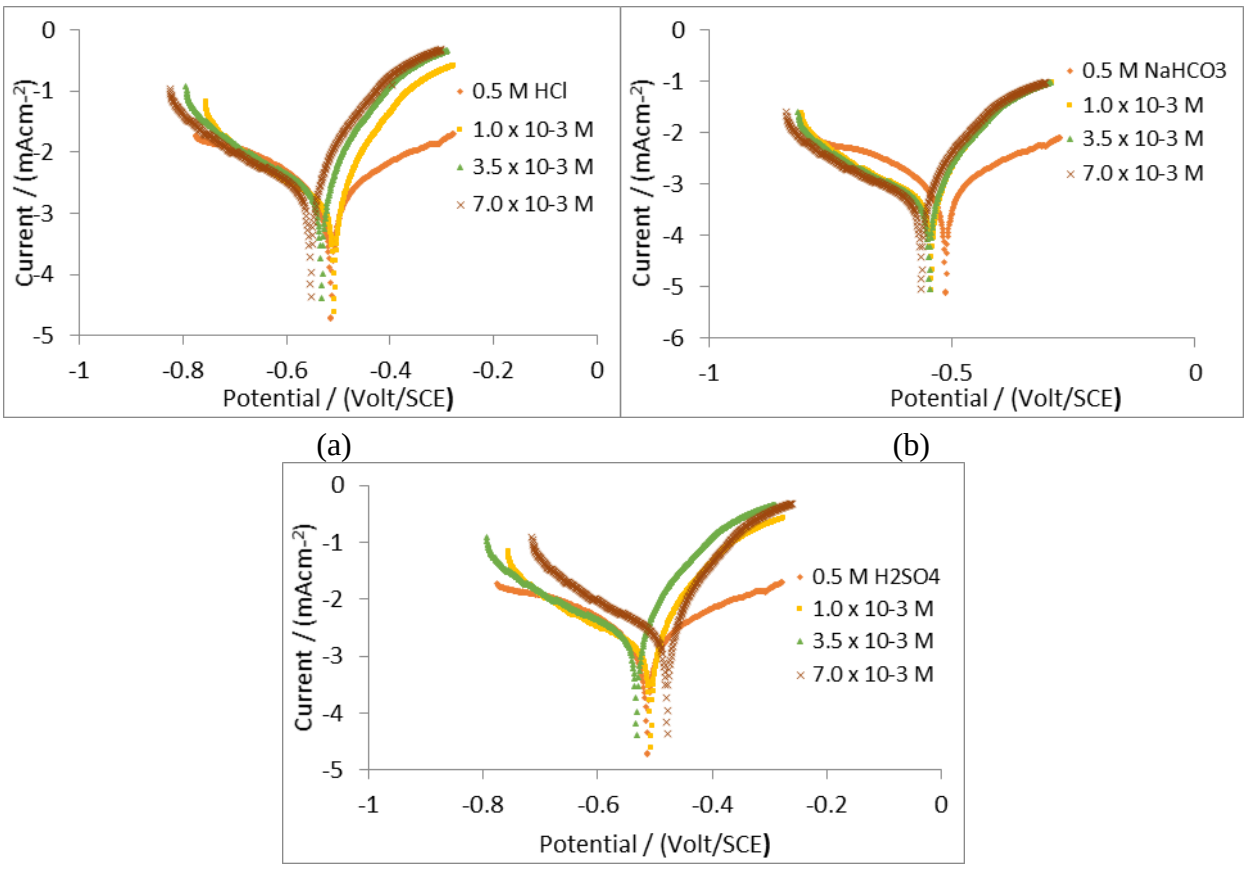

Figure 4. Tafel plots for inhibition of industrial structural steel coupons in 0.5 M (a) HCl, (b) **$NaHCO_3$ and (c) H_2SO_4** solutions.

Table 6: Tafel data showing the extent of inhibition of industrial structural steel coupons in 0.5 M HCl, **$NaHCO_3$ and H_2SO_4** solutions.

	Inhibitor Concentration (mol/L)											
Parameters	0.5 M HCl	1.0 x 10^{-3}	3.5 x 10^{-3}	7.0 x 10^{-3}	0.5 M $NaHCO_3$	1.0 x 10^{-3}	3.5 x 10^{-3}	7.0 x 10^{-3}	0.5 M H_2SO_4	1.0 x 10^{-3}	3.5 x 10^{-3}	**7.0 x 10^{-3}**
I_{corr} (mAcm-2)	3.093	1.073	0.379	0.058	2.190	0.854	0.487	0.142	5.914	2.505	1.663	**0.622**
E_{corr} (mV)	-940	-738	-611	-247	-524	-403.0	-217	-186	-847	-639	-455	**-194**
βc (mV/dec)	1170	928	706	553	1009	917.0	790	683	991	900	783	**688**
βa (mV/dec)	1214	897	515	117	918	800	616	493	1102	1008	865	**765**
IEi (%)	-	65.31	87.75	98.12	-	61.00	77.76	93.52	-	57.64	71.88	**89.48**
Diff. βc (mV/dec)	-	242	464	617	-	92	219	326	-	91	208	**303**
Diff. βa (mV/dec)	-	317	699	1097	-	118	302	425	-	94	237	**337**

3.5 Quantum chemical calculations

Figures 5a - b depict the fully optimized geometry, the HOMO, LUMO and molecular electrostatic potential (ESP) diagrams of the tested expired amiloride molecule. **Figures 5 b - c** shows that the distribution of the HOMO is concentrated in the middle of the molecular structure of the tested molecule. The electronic distribution is mainly located on the aromatic benzene ring, on the oxygen and nitrogen atoms, with less activity around the chlorine atom. Interestingly, the LUMO electron densities of the expired amiloride molecule moved toward the chloride atom and little distribution around the benzene ring**,** suggesting a good electron acceptance ability [22, 26]. The molecular electrostatic potential obtained for the molecule is shown in **Figure 5d**. The most negative regions of the ESP have been given the yellow color, while blue stands for the regions of the most positive ESP. Therefore, the potential increase follows the order blue > yellow. It can be seen that deep yellow color is mainly located over the Benzene ring and over three nitrogen atoms and two other nitrogen atoms beneath, which suggests an interaction with the metallic surface through electrostatic forces [24, 25, 27]. The quantum chemical parameters E_{HOMO} and E_{LUMO}, energy gap (ΔE), electrophilicity index (ω), binding energy, chemical potential, global hardness and softness are presented in **Table 7**. Higher value of E_{HOMO}, lower value of E_{LUMO} are attributed to high metal–inhibitor interactions and therefore high protection efficiency as already observed [21, 26, 27]. More importantly, the energy gap plays a vital function such that the molecule associated with lower ΔE value is also related to high softness, lower hardness, high chemical potential and high binding energy thereby high inhibition ability [22-25]. This was exactly what the research findings revealed of the expired amiloride molecule.

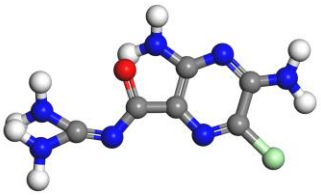

(a)

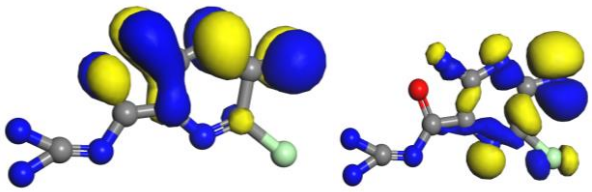

HOMO LUMO

(b) (c)

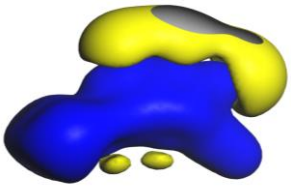

(d)

Figure 5. Depict the (a) fully optimized geometry (b) HOMO (c) LUMO and (d) molecular electrostatic potential diagrams of the amiloride inhibitor on industrial structural steel coupons

Table 7: Quantum chemical descriptors for amiloride molecule on on industrial structural steel coupons

Quantum parameters	**Data (eV)**
E_{HOMO}	-5.54
E_{LUMO}	-5.35
E_{gap} ($E_{HOMO} - E_{LUMO}$)	0.19
Binding energy	-79.63
Chemical potential (μ)	-5.45
Global hardness (η)	0.095
Global softness (S)	5.26
Electrophilicity index (ω)	156.04

3.6. Fukui functions.

The identification of the most reactive sites of the inhibitor is shown in (**Figure 6**). From the condensed fukui functions of the inhibitor where the local reactivity of the molecule is estimated, we have that the maximum positive magnitude of Fukui functions where there is possible nucleophilic attacks is located on C12, C10, C9, C7 and N4. On the other hand, maximum negative magnitudes of Fukui functions are on N15, Cl14, N13, C12, and N11. This implies that the inhibitor has a both higher tendencies to accept and donate electrons hence providing a strong inhibition by molecular adsorption on the metal surface [24, 26-28].

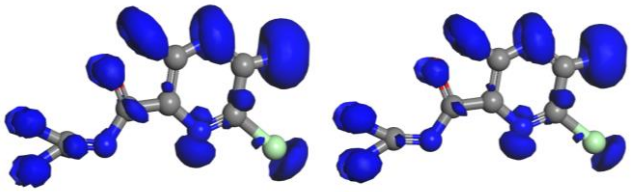

Electrophilic (F-) Nucleuphilic (F+)

Figure 6. Fukui functions showing active sites of amiloride molecules

3.7 Molecular dynamics Simulation analysis

Fig. 7a - e depicts the equilibrium configurations of inhibitor molecules adsorbed on the surface of Fe(110) at different simulated temperatures. As presented in **Fig. 7a – e,** it is probable that the inhibitor molecules are adsorbed on the Fe (110) surface through dinitrobenzene and chloride atom. The energy of adsorption in solution can be calculated following **Equation 16**

$$E_{ads} = E_{total} - \left(E_{surf.+water} + E_{inh.+water}\right) + E_{water} \quad (16)$$

The adsorption energy in the present work were calculated from the average adsorption energy of the obtained equilibrium configurations. The results show that at the investigated temperature (303 K), adsorption energy was negative, therefore, spontaneous adsorption can be deduced [20-21]. This was a confirmation of the already presented result from thermodynamics investigation. Generally, enhanced adsorption between the inhibitor/metal interfaces is always attributed to a more negative value of E_{ads}.

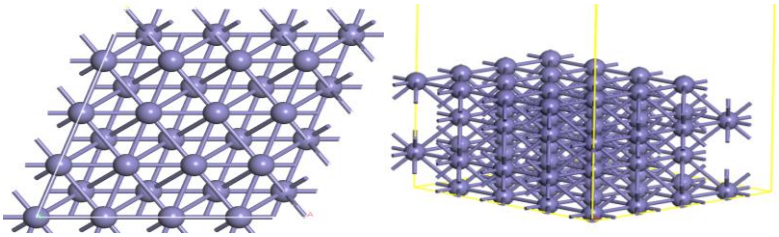

(a) (b)

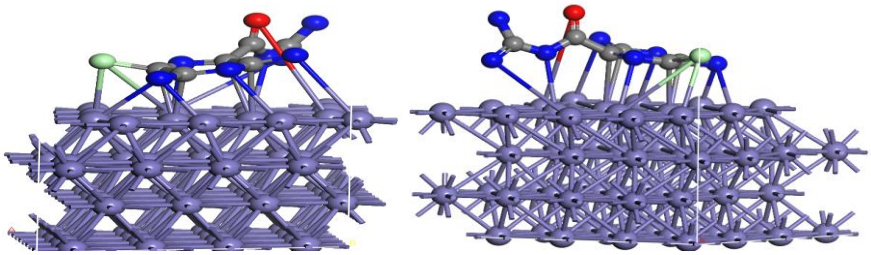

(c) (d)

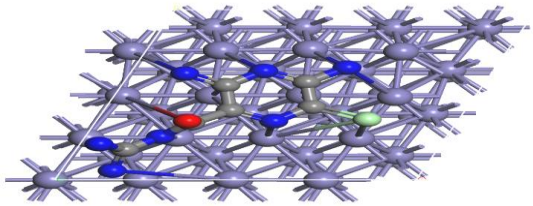

(e)

Figure 7. Simulation diagrams showing (a) optimized Fe (110) bulk surface (onto view), (b) optimized Fe (110) bulk surface (side view), (c) inhibitor adsorption on metal surface (side view 1), (d)) inhibitor adsorption on metal surface (side view 2) and (e)) inhibitor adsorption on metal surface (onto view)

3.8 Adsorption Characteristics

Table 8 described the data for the adsorption of inhibitor molecule on metal surface using the Langmuir adsorption isotherm. The equation for the Langmuir adsorption is shown as **Equation 17**

$$\frac{C}{\emptyset} = \frac{1}{k} + C \qquad (17)$$

where C represented the concentration of inhibitor, k is the equilibrium constant and the surface coverage is Ɵ. The plot of C/Ɵ against Concentration in molL^{-1} (**Fig. 8a - c**) yielded parameters as such as equilibrium (binding) constant, correlation coefficient, slope and adsorption free energy as reported in Table 8. The adsorption free energy as determined from the equilibrium constant of Equation xxx as shown in **Equation 18**.

$$\Delta G = -RT\ln(55.5\ k) \qquad (18)$$

The equilibrium binding constant values were found to be larger and decreasing with concentration of inhibition. This is an indication of high adsorption strength consequence upon strong binding of inhibitor molecule to the metal surface, and a physical adsorption process [25-28]. The correlation coefficient was found not to be greater than unity indication a good fitting of that data to the Langmuir isotherm, hence a monolayer chemical adsorption [13, 28-30]. The slope values were also approximately unity indicating a strong adsorption of the inhibitor. Values of the ΔG_{ads} were negative and more negative than 20 kJmol^{-1}, which explained why the inhibitor reaction will be spontaneous, stabled and physically adsorbed on the metal interface [31-35].

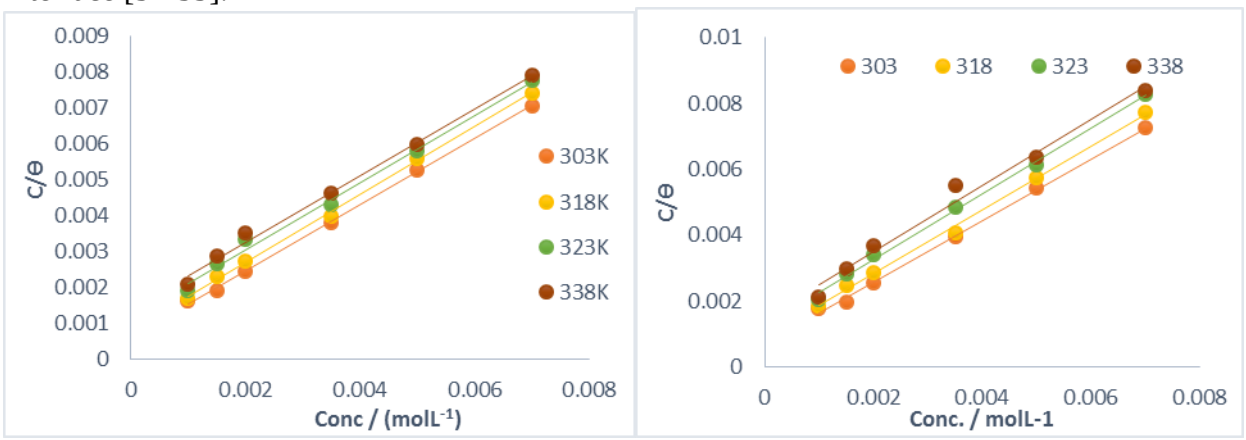

(a) (b)

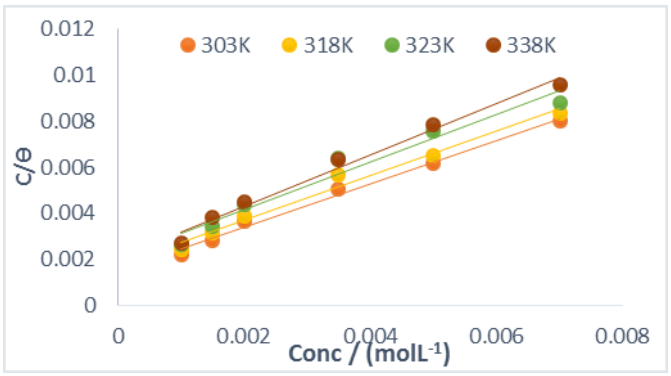

(c)

Figure 8. Langmuir adsorption isotherm for the inhibition of industrial structural steel coupons in 0.5 M (a) HCl, (b) $NaHCO_3$ and (c) H_2SO_4 solutions

Table 8: Langmuir adsorption data for corrosion inhibition of industrial structural steel coupons in 0.5 M HCl, $NaHCO_3$ and H_2SO_4 solutions

	HCl				$NaHCO_3$				H_2SO_4			
Temp.	k	R	ΔG	Slope	k	R	ΔG	Slope	k	R	ΔG	**Slope**
(K)	($molL^{-1}$)		($kJmol^{-1}$)		($molL^{-1}$)		($kJmol^{-1}$)		($molL^{-1}$)		($kJmol^{-1}$)	
303	1.67	0.9992	-11.16	0.9191	1.43	0.9985	-10.78	0.9410	0.67	0.9907	-8.91	**0.9472**
318	1.25	0.9989	-10.97	0.9452	1.11	0.9975	-10.66	0.9683	0.56	0.9821	-8.89	**0.9671**
328	0.83	0.9935	-10.06	0.9333	0.83	0.9964	-10.06	1.0024	0.50	0.9847	-8.73	**1.1228**
338	0.72	0.9946	-10.14	0.9290	0.67	0.9833	-9.940	1.0063	0.48	0.9617	-9.02	**1.0321**

Due to some slope values which were within unity, the data was again fitted to the El-Awady isotherm (**Fig. 9a - c)** to appropriately present the adsorption behavior of the inhibitor onto the steel surface. Equation xxx represent the El-Awady isotherm **equation 19**

$$\log\left(\frac{\emptyset}{1-\emptyset}\right) = \log K + y\log C \ldots \ldots \quad \ldots \quad (19)$$

where y represent the number of inhibitor molecules occupying one active site. Ɵ is the inhibitor surface coverage, C is the concentration, K is the adsorption – desorption equilibrium constant. The value of $\frac{1}{y}$ is the number of active sites occupied by one inhibitor molecule. From **Table 9,** values of $\frac{1}{y}$ were less than unity indicating an approaching multilayer adsorption with each inhibitor molecule attached to a single active site of the metal. Result obtained revealed a possibility of more than one active site being occupied by the inhibitor molecule on the metal surface indicating a strong adsorption [27, 31-32].

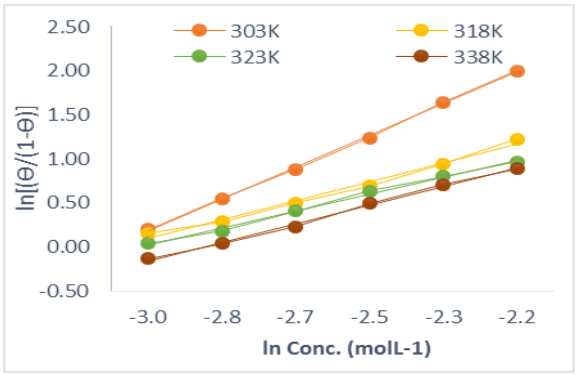

(a)

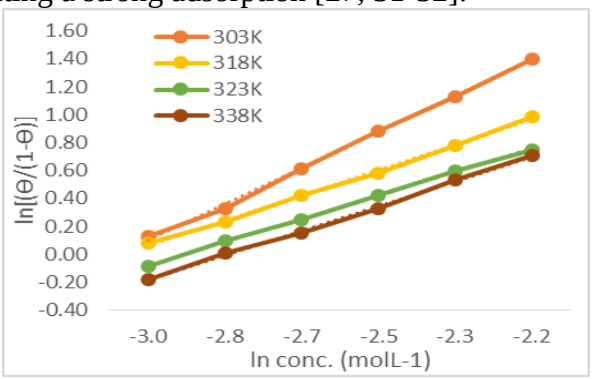

(b)

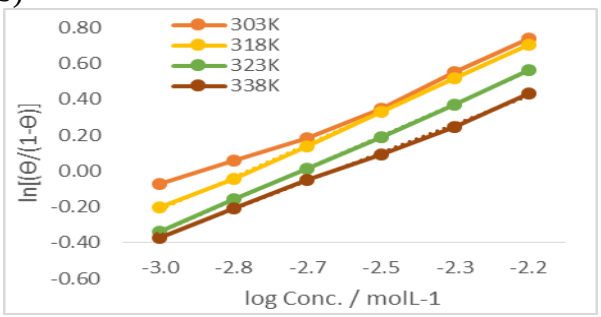

(c)

Figure 9. El-Awady et al adsorption isotherm for the inhibition of industrial structural steel coupons in 0.5 M (a) HCl, (b) $NaHCO_3$ and (c) H_2SO_4 solutions

Table 9: El-Awady et al adsorption isotherm for the inhibition of industrial structural steel coupons in 0.5 M HCl, $NaHCO_3$ and H_2SO_4 solutions

	HCl			$NaHCO_3$			H_2SO_4		
Temp. (K)	1/y	R	ΔG ($kJmol^{-1}$)	1/y	R	ΔG ($kJmol^{-1}$)	1/y	R	ΔG ($kJmol^{-1}$)
303	0.12	0.9863	-15.2	0.12	0.9971	-16.2	0.4	0.9986	-11.73
318	0.17	0.9949	-15.26	0.16	0.9986	-14.45	0.52	0.999	-13.04
328	0.18	0.9992	-14.86	0.25	0.9991	-14.52	0.53	0.9998	-12.53
338	0.36	0.9961	-13.82	0.53	0.9984	-13.08	0.53	0.9986	-13.08

3.9 Thermodynamics investigation

Table 10 recorded the data obtained from the plot of ln Cr against 1/T **(Figure 10a - c)** using the Arrhenius equation as carried by **equation 20 – 22.**

$$Cr = Ae^{-\frac{E_a}{RT}} \quad (20)$$

$$\ln Cr = \ln A - \frac{E_a}{RT} \quad (21)$$

$$\ln Cr = \ln A - \frac{E_a}{R}\frac{1}{T} \quad (22)$$

where E_a is the activation energy, A is the binding constant, Cr the corrosion rate of metal, R is the gas constant and T the absolute temperature. E_a expresses the difficulty of the amiloride molecules' movement from one position to another, which is controlled by the intermolecular forces, bulkiness and rigidity [33-36].

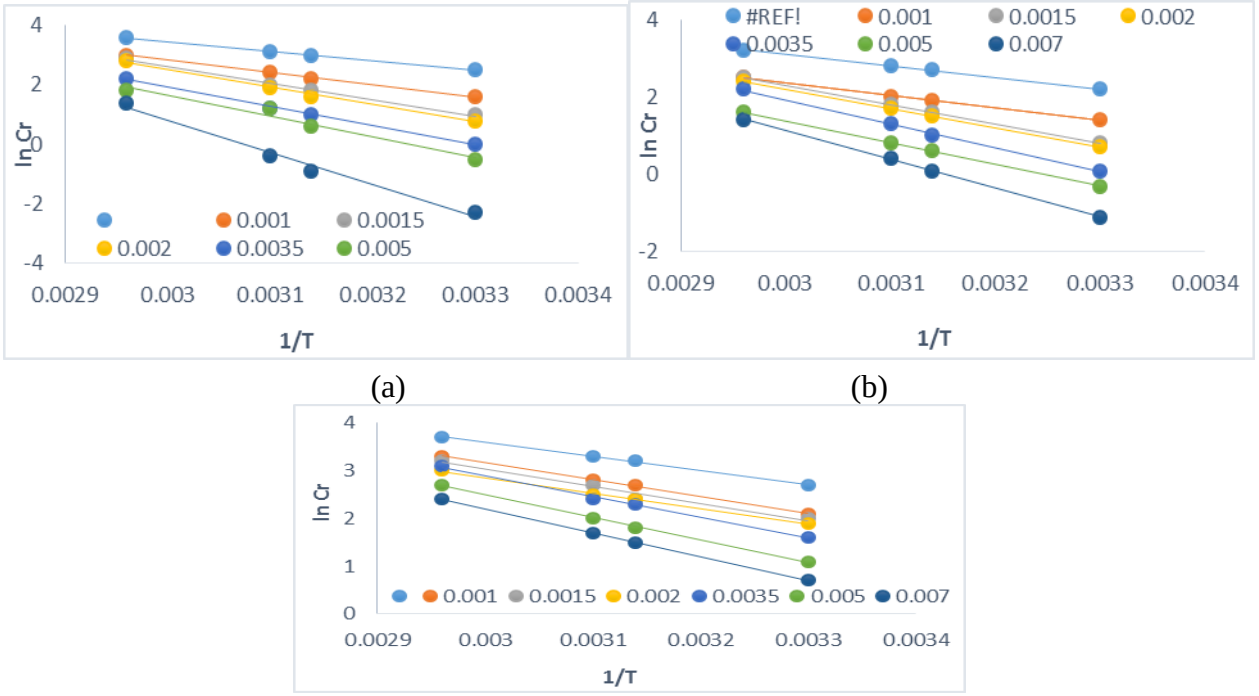

(a) (b)

(c)

Figure 10. Arrhenius plots for the inhibition of industrial structural steel coupons in 0.5 M (a) HCl, (b) $NaHCO_3$ and (c) H_2SO_4 solutions

It was observed that the values of activation energy were larger in the amiloride inhibited solution compared to the free solution indicating that the inhibitor was well adsorbed on the metal coupons by overcoming the difficulty in molecular movement posed by intermolecular forces, bulkiness and rigidity of solution [30, 37-38]. This is confirmed by the larger values from the free exponential factor (A) in inhibited solution which indicates that the frequency of the effective molecular collision of the inhibitors had the proper orientation between particles and appropriate temperature for inhibition – surface reaction to occur [12, 19-21, 39]. A physical adsorption that is followed by a chemical adsorption was interpreted from the E_a data seen to be slightly greater than 20 kJmol^{-1} also describing a stronger adsorption of the amiloride inhibitor.

The Erying transition state equation given in **equation 23** was adopted for the graphical determination of both the enthalpy and entropy of adsorption using the thermometric data that evolved from the experimental analysis.

$$\ln\frac{k}{T} = -\frac{\Delta H}{R}\frac{1}{T} + \ln\frac{kB}{h} + \frac{\Delta S}{R} \qquad (23)$$

where k is the rate constant, T is the absolute temperature, ΔH is the enthalpy of adsorption, ΔS is the entropy of adsorption, kB is the Boltzman constant, h is the plank constant and R, the universal gas constant. The values for ΔH and ΔS can be determined from kinetic data obtained from a $ln\frac{k}{T}$ vs. $\frac{1}{T}$ plot as seen in **Figs 11a – c**. The straight line with negative slope. $-\frac{\Delta H}{R}$, and a y-intercept, $ln\frac{kB}{h} + \frac{\Delta S}{R}$ from the equation gives the two major thermodynamic parameters investigated **(References)**. Values of enthalpy of adsorption were less than 80 kJmol^{-1} and positive (**Table 10)**, which is an indication of a possible physical adsorption phenomenon and endothermic reaction process implying that heat was absorbed into the system in the process of reaction, hence breaking up the bonds necessary for corrosion reaction and enhancing inhibition [29-30, 39-40]. The entropy of adsorption was negative describing a dissociation and a lower amount of disorder meaning that they inhibitors therefore reduce the amount of kinetic energy established in the system hence reducing the excitation of the molecules and amount of random activity [40-43].

Table 10: Thermodynamic/Kinetic data for the inhibition of industrial structural steel coupons in 0.5 M HCl, $NaHCO_3$ and H_2SO_4 solutions

	HCl				NaHCO3				H2SO4			
Inh. Conc.	A Lmol^{-1}s^{-1}	Ea kJ/mol	ΔH kJ/mol	ΔS kJmol^{-1}	A Lmol^{-1}s^{-1}	Ea kJ/mol	ΔH kJ/mol	ΔS kJmol^{-1}	A Lmol^{-1}s^{-1}	Ea kJ/mol	ΔH kJ/mol	**ΔS kJmol^{-1}**
Blank(0.5 M)	13.1	26.8	7.360	-215.63	11.9	21.4	7.150	-215.42	12.4	24.4	7.51	**-215.78**
1.0 x 10^{-3} M	15.2	34.3	17.77	-226.04	12.0	26.8	9.99	-218.26	12.5	26.8	11.97	**-220.24**
1.5 x 10^{-3} M	19.3	46.2	30.38	-238.65	17.2	41.6	24.22	-232.49	13.7	29.3	11.97	**-220.24**
2.0 x 10^{-3} M	20.2	48.9	31.58	-239.85	17.3	41.6	24.64	-232.91	13.7	29.6	12.11	**-220.38**
3.5 x 10^{-3} M	21.2	53.5	36.61	-244.88	18.1	46.4	29.25	-237.52	16.0	36.4	21.32	**-220.59**
5.0 x 10^{-3} M	22.4	57.4	39.09	-247.36	20.5	51.4	36.40	-244.67	16.0	39.1	24.29	**-232.56**
7.0 x 10^{-3} M	33.4	63.1	76.34	-284.61	23.2	61.2	44.05	-252.32	17.2	41.6	26.56	**-234.83**

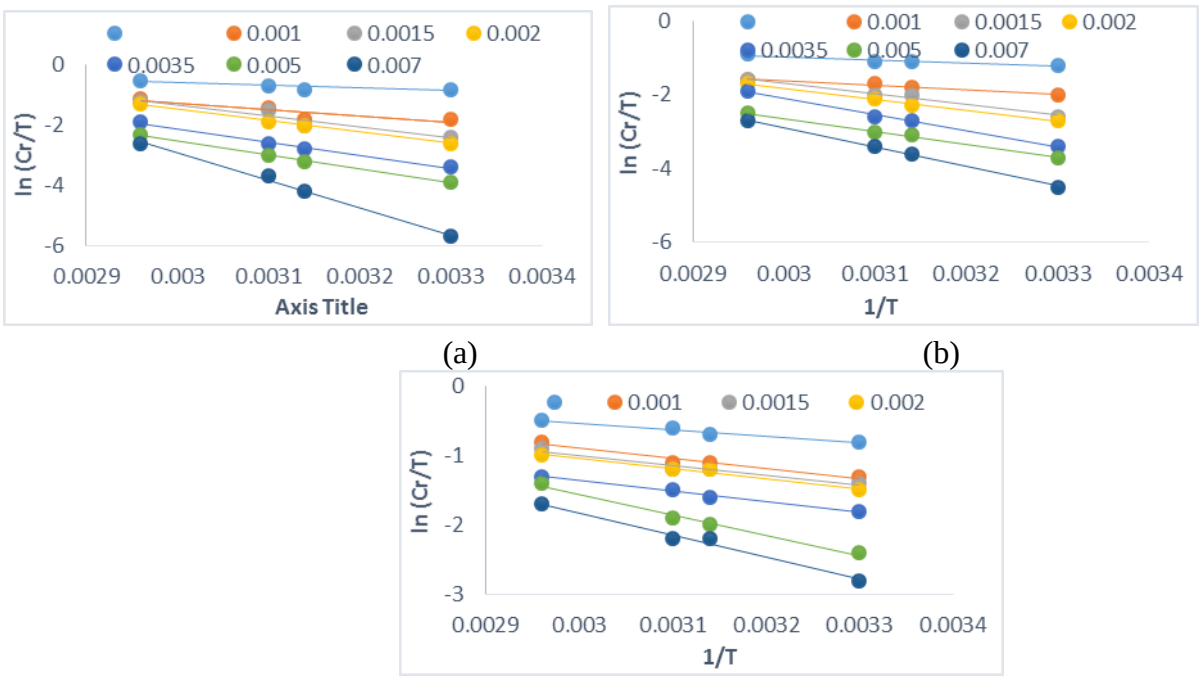

Figure 11. Transition state plots for the inhibition of industrial structural steel coupons in 0.5 M (a) HCl, (b) **$NaHCO_3$ and (c) H_2SO_4** solutions

3.10 Scanning electron microscopic examination

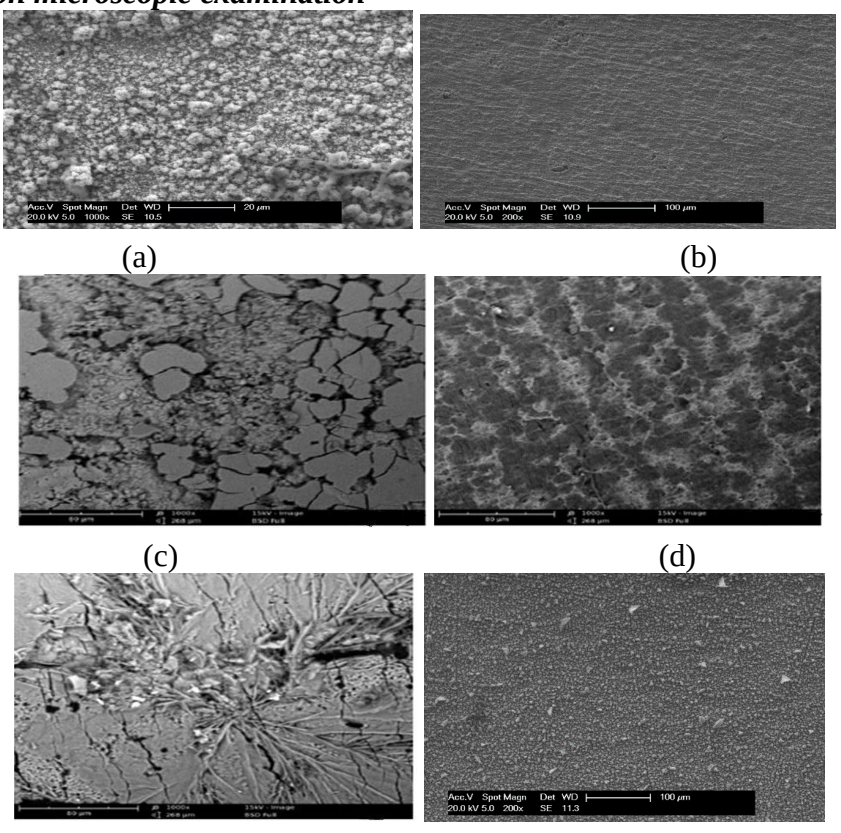

Figure 12. Micrographs of industrial structural steel coupons in (a) free HCl and (b) 7.0 x 10^{-3} M amiloride inhibitor, (c) free $NaHCO_3$ and (b) 7.0 x 10^{-3} M amiloride inhibitor, (a) free H_2SO_4 and (b) 7.0 x 10^{-3} M amiloride inhibitor using SEM.

Fig. 12a - f shows the micrographs for the metal coupons in different free solutions and highest inhibitor concentration (7.0×10^{-3} M) through the aid of scanning electron microscopy (SEM). In all the different free solutions, there was a complete destruction of the metal surface indicating the inability of the metal surface to withstand the free acid and alkaline solutions [44-46]. The case was different when inhibitor was added, we saw the efficacy of the inhibitor through protection of the surface from damage consequence upon adsorption of molecules of amiloride through the active sites of the metallic surface, resulting in a smoother surface (except for a few spots), signifying the protection of the metal from corrosion [47-49].

Conclusion

1. The research so far carried out proved expired amiloride drug as a good inhibitor for industrial structural steel in all the tested media but with the following efficacy progression: $H_2SO_4 < NaHCO_3 < HCl$.
2. Inhibition of corrosion in industrial structural steel was by molecular adsorption on metal surface leading to formation of a stronger intermolecular force of attraction at the inhibition-metal interface.

3. Electrochemical data were in strong agreement with the chemical data as the expired amiloride drug increased the charged transfer resistance, reduced both the double layer capacitance and corrosion current densities of the interface.
4. A monolayer chemical adsorption was deduced from the research carried out as data fitted very well to the Langmuir adsorption isotherm while a physical adsorption mechanism was deduced from the decreasing values of the equilibrium constant.
5. It was also gathered from the thermodynamic calculations that the inhibitor was stabled, spontaneous, physically adsorbed and presented minimal degree of disorderliness.
6. Theoretical data was in agreement with experimental result in terms of adsorption at reactive sites in the metal steel. The entire results describing the efficiency of the inhibitor in various test media was confirmed by the micrographs from SEM.

References

[1]. R.R. Pierre, Handbook of Corrosion Engineering, McGraw-Hill Pub., New York, 2015.
[2]. B.N. Popov, Corrosion engineering principles and solved problems, Elsevier, Netherlands, 2015.
[3]. R.K. Pathak, P. Mishra, P. Mishra, *International Journal of Science and Research*, 5(4) (2016) 671-677.
[4]. U. Bharatiya, P. Gal, A. Agrawal, M. Shah, A. Sircar, *Journal of Bio- and Tribo-Corrosion*, 5 (2019) 1-5.
[5]. C. Verma, D. S. Chauhan, M. A. Quraishi, *J. Mat. Env. Sc.*, 8(11) (2017) 404 – 405
[6]. B. A. Suraj, N. V. Shitole, S. M. Lonkar, *Journal of Chemical and Pharmaceutical Research*, 6(7) (2014) 1865-1872
[7]. N. Nnaji, N. Nwaji, J. Mack, T. Nyokong, *Molecules*, 24(1) (2019) 207.doi: 10.3390/molecules24010207
[8]. C. Verma, L. O. Olasunkanmi, E. E. Ebenso, M. A. Quraishi, *J. Mol. Liq*. 251 (2018) 100–118.
[9]. N. C. Ngobiri, E. E. Oguzie, N. C. Oforka, O. Akaranta, *Arabian Journal of Chemistry*, 12 (2019) 1024-1034.

[10]. K. Boumhara, H. Harhar, M. Tabyaoui, A. Bellaouchou, A. Guenbour, A. Zarrouk, *Journal of Bio- and Tribo-Corrosion*, 5 (2019) 1-8
[11]. I. A. Adejoro, C. U. Ibeji, D. C. Akintayo, *Chem Sci J*, 8 (2017) 149. doi: 10.4172/2150-3494.100014
[12]. I. Danaee, S. RameshKumar, M. RashvandAvei, M. Vijayan, *Mat. Res*. 23(2) (2020) https://doi.org/10.1590/1980-5373-mr-2018-0610
[13]. K. A. Salima, B. A. Wassan, A. K. Anees, *International Journal of Industrial Chemistry*, 10 (2019) 159–173
[14]. M. AbdallahaI, S. O. Zaafarany, A. A. Al-Karanee, El-Fattaha, *Arabian Journal of Chemistry*,5(2) (2012) 225-234
[15]. I. A. Akpan, N. o. Offiong, *Indian Journal of Chemical Technolgy*, 24 (2017) 107 – 110
[16]. D. Dwivedi, K. Lepkova, T. Becker, *RSC Adv*. 7 (2017) 4580–4610. doi: 10.1039/C6RA25094G
[17]. D. K. Verma, *Chemistry and Materials Research* , 7(5) (2015) 69 – 76
[18]. A. S. Fouda, M. Eissa, El-Hossiany, *Int. J. Electrochem. Sci.*, 13 (2018) 11096–11112, doi:10.20964/2018.11.86
[19]. A. Salhi, A. Bouyanzer, I. El Mounsi, H. Bendaha, A. Chetouani, H. Amhandi, A. Zarrouk, B. Hammouti, J. M. Desjobert, J. Costa, *Mor. J. Chem.*, 4(4) (2016) 1037 - 1051
[20]. N. Asadi, M. Ramezanzadeh, G. Bahlakeh, B. J. Ramezanzadeh, *Taiwan Inst. Chem. Eng.*, 95 (2019) 252–272.
[21]. S. Dahiya, N. Saini, N. Dahiya, H. Lgaz, R. Salghi, S. Jodeh, S. Lata, *Port. Electrochim. Acta*, 36(3) (2018) doi.org/10.4152/pea.201803213
[22]. M. T. Majda, M. Ramezanzadeh, B. Ramezanzadeh, G. Bahlakeh, *Journal of Hazardous Materials*, 382 (2020) 1-16.
[23]. O. Dagdag, A. El Harfi, O. Cherkaoui, Z. Safi, L. G. Wazzan, E. D. Akpan, *RSC Advances*, 9 (2019) 4454-4462.
[24]. M. Yadav, S. Kumar, N. Kumari, I. Bahadur, E. E. Ebenso, *International journal of electrochemical science*, 10 (2015) 602 – 624.
[25]. B. Evgeniji, R. J. Macdonald, R.J. Impedance, Spectroscopy, Theory and Experiment. 2nd ed. John Wisley and Son Pub., Canada, 2000
[26]. B. M. Prasanna, B. M. Praveen, H. Narayana, T. V. Venkatarangaiah, C. T. Harmesh, *Ind. Eng. Chem. Res.*, 53 (20) (2014) 8436–8444
[27]. R. Narasimha, *International Journal of Chemistry and Materials Research*, 6(1) (2018) 1-7 DOI: 10.18488/journal.64.2018.61.1.7
[28]. M. Shahraki, S. M. Habibi-Khorassani, M. Noroozifar, Z. Yavari, M. Darijani, M. Dehdab, *Iranian Journal of Materials Science & Engineering*, 4(4) (2017). DOI: 10.22068/ijmse.14.4.35
[29]. K. Bouayad, Y. Kandi Rodi, E. H. El Ghadraouni, H. Elmsellem, Y. Ouzidan, B. El Mahi, E. M. Essassi, I. Abdel-Rahman, A. Chetouani, B. Hammouti, *Mor. J. Chem*., 5(2) (2017) 285 - 296
[30]. E. Alibakhshi, M. Ramezanzadeh, G. Bahlakeh, B. Ramezanzadeh, M. Mahdavian, Motamedi, D. A. Al-Shehri, *Sustainability*, 11 (8) (2019) 1-18.
[31]. A. Singh, K. S. Ashish, M. A. Quraishi, *The Open Electrochemistry Journal*, 2 (2010) 43-51
[32]. K. F. Khaled, A. M. El-Sherik, *International Journal of Electrochemical Science*, 8 (2013) 10022 – 10043

[33]. F. Abeng, M. Ikpi, K. Uwakwe, G. Ikpi, *International Research Journal of Pure & Applied Chemistry, 15(3) (2017) 1-12*
[34]. A. Singh, K. R. Ansari, D. S. Chauhan, M. A. Quraishi, H. Lgaz, I. M. Chung, *J. Colloid Interface Sci*. 560 (2020) 225–236.
[35]. P. O. Ameh, N. O. Eddy, *Cogent Chemistry*, 2 (2016) 125.
[36]. A. S. Fouda, K. E. Shalabi, A. Hossiany, *J Bio Tribo Corros*, 2 (2016) 18. https://doi.org/10.1007/s40735-016-0048-x
[37]. P. O. Ameh, N. O. Eddy, *Protection of metals and physical chemistry of surfaces,* (2018) 1- 13.
[38]. K. F. Khaled, N. A. Al-Mobarak, *International. Journal of Electrochemical Science*, 7 (2012) 1045 – 1059
[39]. P. Geethamani, P. K. Kasthuri, *Cogent Chemistry*, 1 (2015) http://dx.doi.org/10.1080/23312009.2015.1091558
[40]. I. Hussin, R. S. Al-Shafey, F. A. Abdel Hameed, A. S. Ali, M. S. Aboul-Magd, *Int. J. Pharm. Sci. Rev. Res*., 27(1) (2014) 146-152
[41]. A. S. Fouda, M. A. El Morsi, T. El, *J Anal Pharm Res.*, 5(5) (2017) 00153. DOI: 10.15406/japlr.2017.05.00153
[42]. K. F. Khaled, *Corrosion Science*, 52 (2010) 2905 – 2916
[43]. Y. El aoufir, Y. El Bakri, Kerroum, H. Lgaz, A. Harmaoui, A. Chefouani, J. Sebhaoui, R. Salghi, Y. Ramli, A. Guenbour, E. M. Essassi, H. Oudda, *Mor. J. Chem.*, 5(4) (2017) 545 - 559
[44]. P. Singh, S. C. Dheeraj, K. Srivastava, V. Srivastava, M. A. Quraishi, *International Journal of Industrial Chemistry,* 8(4) (2017) 363-372. DOI: 10.1007/s40090-017-0120-5
[45]. A. S. Fouda, M. A. El Morsi, T. El Mogy, *Green Chemistry Letters and Reviews*, 10 (4) (2017) 336-345
[46]. I. A. Akpan, N. O. Offiong, *International Journal of Chemical and Process Engineering Research*, 1(2) (2014) 10-18
[47]. M. Z. H. M. A. Aziz, M. R. Hasan, M.R. *Anti-Corrosion Methods and Materials*, 63 (4) (2016) 308-315. https://doi.org/10.1108/ACMM-11-2015-1597
[48]. P. O. Ameh, P. Ukoha, P. Ejikeme, N. O. Eddy, *Ind Chem.*, 2 (2016) 119. doi: 10.4172/2469-9764.1000119
[49]. H. Lgaz, S. K. Saha, A. Chaouiki, K. S. Bhat, R. Salghi, P. Banerjee, I. H. Ali, M. I. Khan, I. M. Chung, *Constr. Build. Mater.* 233 (2020) 117320